Thermomechanical Fatigue, Oxidation, and Creep: Part II. Life Prediction

R.W. NEU and HUSEYIN SEHITOGLU

A life prediction model is developed for crack nucleation and early crack growth based on fatigue, environment (oxidation), and creep damage. The model handles different strain-temperature phasings (*i.e.*, in-phase and out-of-phase thermomechanical fatigue, isothermal fatigue, and others, including nonproportional phasings). Fatigue life predictions compare favorably with experiments in 1070 steel for a wide range of test conditions and strain-temperature phasings. An oxide growth (oxide damage) model is based on the repeated microrupture process of oxide observed from microscopic measurements. A creep damage expression, which is stress-based, is coupled with a unified constitutive equation. A set of interrupted tests was performed to provide valuable damage progression information. Tests were performed in air and in helium atmospheres to isolate creep damage from oxidation damage.

I. INTRODUCTION

A. *Background*

LIFE prediction models are needed to assist with the design and evaluation of components undergoing thermomechanical fatigue (TMF). The models currently available are severely limited in their generality. Often the application of the current models outside the range of experiments used to derive the model is not recommended. Since the mechanisms producing damage may differ from one set of testing conditions to another, advancement in the area of life prediction needs to be in the identification of these different damage mechanisms and the conditions which activate them. Microstructure and bulk parameters which quantify these mechanisms should be established. The model derived in this report attempts to take advantage of physical damage measurements and identifies these with a measure of lifetime.

There have been data reported for isothermal fatigue tests; however, many critical components undergo a complicated temperature-strain history which can be more closely approximated by a TMF test in the laboratory.[1] Therefore, it is important that the new generation of life prediction models is able to handle these strain-temperature histories and yet remain general enough so that the prediction model is not restricted to only a few temperature, strain rate, or strain range levels.

When elevated temperature experiments are conducted, environmental and creep effects on the life can become significant, depending on the material and testing parameters. Both environmental effects and creep are activated simultaneously with fatigue and lower the life. These damage mechanisms change with strain, temperature, phasing, and strain rate in a complicated way, as indicated in Part I. In most cases, the strain-temperature variation with time and the material condition will dictate which mechanism is the most damaging.

R.W. NEU, Research Assistant, and HUSEYIN SEHITOGLU, Associate Professor, are with the Department of Mechanical and Industrial Engineering, University of Illinois, Urbana, IL 61801.

Manuscript submitted May 16, 1988.

B. *Current Life Prediction Models for High-Temperature Fatigue*

1. *Oxidation-fatigue models*

The earliest life prediction model on environmental effects is the frequency-modified strain-life equation[2] which included, in addition to the plastic strain range, a frequency factor which accounted for the effect of oxidation. The early work on oxidation-fatigue interaction considered the effect of hold times on lifetime under isothermal fatigue conditions. These life prediction models are configured to handle either "crack initiation or crack growth to a certain size" with modified low cycle fatigue equations or "crack growth" with modified fracture mechanics parameters. The structures of these models are discussed here.

Challenger *et al.*[3] developed a model which predicts the cycles to initiate a surface oxide crack. No creep effects for the 2.25 Cr-1Mo alloy steel at 593 °C were included. In the absence of hold times, the oxidation effect changes with strain rate (or frequency), and this was not considered in the model. Using the parabolic oxidation law to characterize oxidation of surface-connected grain boundaries in RENÉ 80,* Antolovich *et al.*[4,5] were able to derive a fatigue-life equation. The initiation fatigue lives were shown to decrease linearly with total cycle period and with hold times. Along a similar approach, Reuchet and Rémy[6] developed a model by recognizing the accelerated oxide growth rate with increasing applied strain range. The total crack growth is the sum of the crack advance due to the fatigue process and due to the environmental process (established by metallographic measurements). This is, in principle, also similar to the approach of Skelton and Bucklow.[7]

*RENÉ is a trademark of the General Electric Company.

Saxena and Bassani's[8] interest was in growth of long cracks; therefore, they proposed an oxidation-modified crack growth law involving ΔK. Kinetics of oxidation (parabolic) at crack tips was included in the model. The model predicted that the growth rate due to oxidation increased with hold time to one-half power. The model was tested for several steels and Ni-based superalloys

and provided satisfactory correlation. Liu and Oshida[9] have a model similar to Saxena and Bassani's; however, they predict a linear dependence of growth rate with hold times or with strain rate.

To better understand the effect of the environment, some investigators[10–15] have performed tests in inert gas environments or in vacuum and compared these to tests performed in air or other oxidizing environments.

Attempts have been made to predict thermomechanical fatigue behavior based on isothermal behavior;[11,16,17] however, the oxidation-induced damage micromechanisms occurring during a TMF cycle can be different from an isothermal cycle. Furthermore, the question of which isothermal temperature should be used to predict TMF data based on isothermal fatigue data is not resolved. Some critical TMF tests should be performed, including experiments where oxidation damage is eliminated with environmental control. These tests and isothermal tests at different strain rates will be shown to be sufficient to build a consistent model which resolves many of these issues.

2. *Creep-fatigue models*

The problem of simultaneous creep fatigue has been addressed in earlier work. The strain range partitioning method[18] and time-cycle fraction rule (adopted as an ASME code[19]) were developed to handle plastic and creep strains on life. A modified time-cycle fraction rule has been used with applications to cumulative damage and may be found in References 20 through 25.

Many researchers have considered creep fatigue to be a propagation-controlled problem, where the damage micromechanism considered is assumed to influence the fatigue crack growth or *vice versa*. Majumdar and Maiya[26] considered the influence of creep cavity growth ahead of a crack growing by fatigue in their damage-rate equations. In their model, it is assumed that sintering of cavities occurs in compression, effectively reversing the creep damage occurring in tension. These damage-rate equations have recently been applied to TMF loadings.[27]

In crack propagation-controlled models, the creep damage in a material is bounded by two extremes.[28] When no creep damage is present, the damage at the crack tip is given by the plastic zone size; when creep damage is extensive, it is assumed that the plastic creep zone ahead of the crack in the bulk of the material controls damage growth.[28] This model is analogous to the use of a crack tip displacement parameter to characterize fatigue-creep crack growth.[29]

Cavity formation ahead of a crack tip modifies the crack tip stress fields; therefore, modified fracture mechanics parameters have been used[8,9,30] to handle fatigue-creep crack growth. In the absence of cavities, the crack tip stress/strain fields are still modified.[31] Other micromechanisms which have been considered in creep-fatigue interactions include intergranular damage (nucleation and growth of grain boundary cavities without aid from a major crack),[32,33] growth of small cracks,[14] and models for grain boundary sliding.[34,35,36]

Experiments are needed to isolate the fatigue-creep effects from the oxidation effects, allowing the constants in the creep damage term to be formulated directly. This could be accomplished by performing tests in a helium environment, which eliminates oxidation damage and thus isolates the creep damage from the environmental damage. These types of experiments were conducted and were discussed in Part I.

C. *Current Work*

A life prediction model is developed. Specifically, the model (a) accounts for oxide rupture at surface and at crack tips; (b) accounts for intergranular damage observed in conditions where creep damage is dominant; and (c) handles arbitrary strain-temperature histories (phasing). Illustrated in Figure 1 are the phasings considered in current tests on 1070 steel. The phasings in Figure 1 are all proportional, which means $\dot{\epsilon}_{th}/\dot{\epsilon}_{mech}$ remains constant throughout the cycle.

II. LIFE PREDICTION METHODOLOGY

A. *Damage Mechanisms*

Consider that three possible damage mechanisms exist: (1) fatigue, (2) environmental attack (oxidation), and (3) creep. Depending on the temperature, strain, and phasing, all three of these damage mechanisms could be operating. If the temperature is too low for significant oxidation and creep, the fatigue damage mechanism will control the life. In an out-of-phase TMF test on the material considered (in which the high temperatures coincide with compressive stress), oxidation damage can be significant, while creep damage is negligible, since void

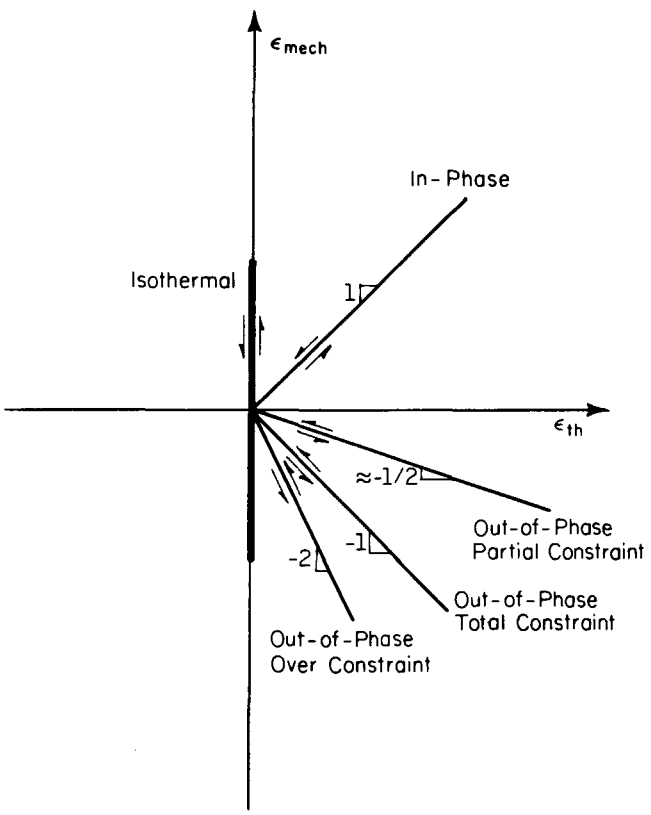

Fig. 1—Schematic showing the strain-temperature histories considered in the 1070 steel testing program.

growth and intergranular cracking mechanisms are suppressed in compression. In this case, the life will be governed by the oxidation damage mechanism.

In the model, the damage per cycle from these three mechanisms is summed to obtain a total damage per cycle, D^{tot}:

$$D^{tot} = D^{fat} + D^{ox} + D^{creep} \quad [1]$$

where the superscripts "fat," "ox," and "creep" represent fatigue, oxidation, and creep, respectively. Without prior knowledge of the most damaging mechanisms for a given strain-temperature history, this equation will predict the total damage.

Equation [1] may be rewritten in terms of the failure life, N_f, since damage is equal to $1/N_f$ (assuming linear damage and damage is equal to 1 at failure).

$$\frac{1}{N_f} = \frac{1}{N_f^{fat}} + \frac{1}{N_f^{ox}} + \frac{1}{N_f^{creep}} \quad [2]$$

The discussion of these damage terms follows. The fatigue damage term is represented by the strain-life equation[37] and is discussed in the next section. The discussion and development of the oxidation and creep damage terms are more involved, and each is considered in a separate section. The model constants will be described for 1070 steel, but the model would be applicable to other materials.

B. *Fatigue Damage Term*

Fatigue damage is represented by classical fatigue mechanisms which normally occur at ambient temperatures. These include "to-and-fro" slip of dislocations and the formation of a crack. Crack growth occurs by localized deformation and slip in the cyclic plastic zone ahead of the crack tip. Most of the tests in this study are performed at elevated temperatures where many variables (strain range, strain rate, temperature, and strain-temperature phasing) may affect the life. However, the "fatigue" mechanism (involving crack nucleation and early crack growth) is assumed to be governed by mechanical strain range, $\Delta\varepsilon_{mech}$. The plastic strain range component of $\Delta\varepsilon_{mech}$ may also be utilized; however, for many loading conditions, including thermal loading, its determination requires further calculations. The use of total strain range is simpler and equally as relevant as plastic strain range.

The fatigue-life term, N_f^{fat} (hence, $D^{fat} = 1/N_f^{fat}$), is estimated from the strain-life relation:[37]

$$\frac{\Delta\varepsilon_{mech}}{2} = \frac{\sigma_f'}{E}(2N_f^{fat})^b + \varepsilon_f'(2N_f^{fat})^c \quad [3]$$

where σ_f' is the fatigue strength coefficient, E is Young's modulus, b is the fatigue strength exponent, ε_f' is the fatigue ductility coefficient, and c is the fatigue ductility exponent.

The constants (E, σ_f', b, ε_f', and c) are determined from isothermal room-temperature fatigue tests and are given in Reference 38. In Figure 2, the room temperature (20 °C) isothermal strain-life curve for 1070 steel is shown along with other 1070 steel data, which would also be expected to have a life based solely on N_f^{fat}. These include isothermal tests performed at or below 400 °C, where little or no oxidation and creep occur, and 600 °C isothermal helium tests performed at a high strain rate ($\dot{\varepsilon} = 0.02\ s^{-1}$), which eliminates oxidation effects and minimizes creep effects.

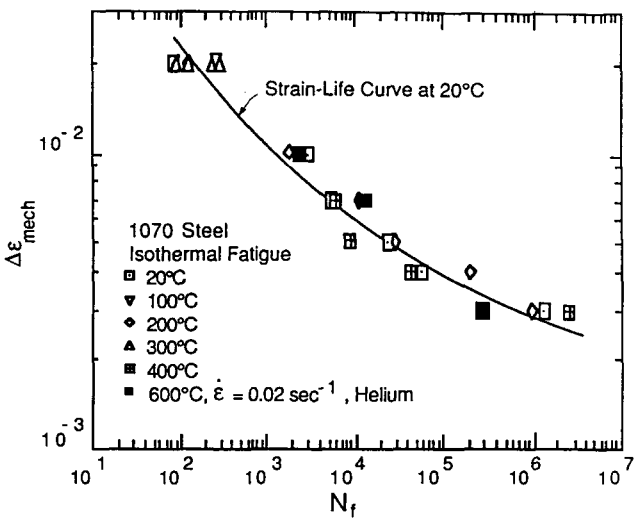

Fig. 2—Strain-life curve at 20 °C for 1070 steel with test results which have a life governed by fatigue damage only.

The room temperature strain-life curve can be considered an upper bound on life. The lives of all tests performed with this material were found to be less than or approximately equal to the room temperature tests. Any decrease in life can be attributed to D^{ox}, D^{creep}, or both.

In cases where crack growth outside the size of the specimen has to be considered, the fatigue life includes a long crack propagation period which is determined using fracture mechanics or modified fracture mechanics parameters.[8,9,30] Crack growth experiments would result in determination of N_f^p, long crack propagation life. Then,

$$N_f^{tot} = N_f + N_f^p \quad [4]$$

where N_f is determined by the proposed model and N_f^{tot} represents both specimen life (initiation and crack growth to a certain size) and long crack propagation life.

III. OXIDATION DAMAGE TERM

A. *Oxidation-Induced Crack Growth Model*

A damage model is proposed which reflects the oxidation-induced crack nucleation and growth as observed in the micrographs and described in Part I. Oxidation-induced crack growth is described as the repeated formation of an oxide layer at the crack tip and its rupture, exposing fresh metallic material to the environment. Crack nucleation is defined as the rupture of the first oxide layer formed.

1. *Type I growth*

The formation of an oxide intrusion by the process of oxide rupture is illustrated by Figure 3. Initially, an oxide layer forms on the surface (a). When this oxide layer reaches a critical thickness, h_{f1}, the oxide ruptures, and

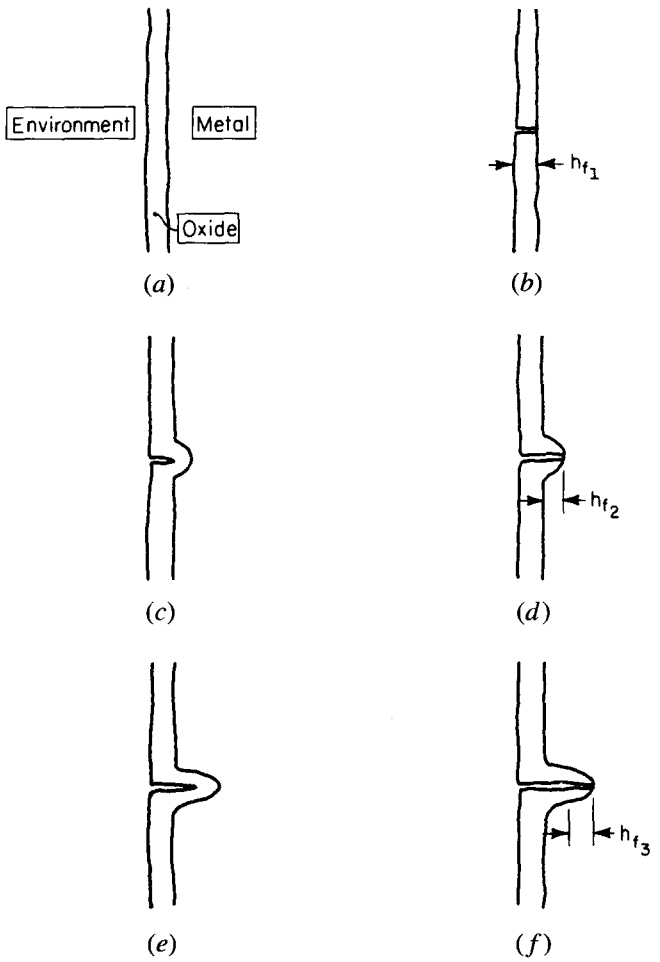

Fig. 3—Schematic showing the nucleation of Type I oxide growth.

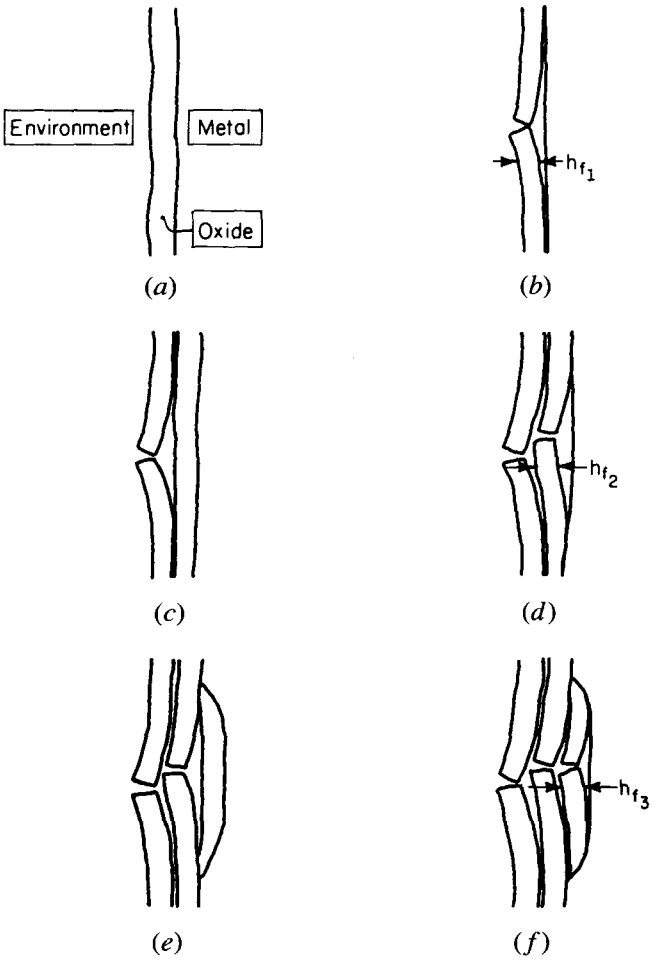

Fig. 4—Schematic showing the nucleation of Type II oxide growth.

crack nucleation has occurred (b). Then a fresh metallic surface is exposed to the environment which rapidly oxidizes (c). When the thickness of this newly formed oxide reaches h_{f2}, the oxide again ruptures (d). The process continues, as shown in Figures 3(e) and (f). Note that the critical thickness when rupture occurs does not have to be constant but may change with applied strain range, strain rate, and temperature.

Type I growth is characterized by a "continuous" oxide layer. A "continuous" oxide layer results in oxide intrusions with no visible stratification in the oxide. This will be distinguished from Type II growth which is characterized by "multilayer" or "stratified" oxide growth, which has been observed by other researchers.[7,38–41]

2. *Type II growth*

A schematic illustrating Type II growth is given in Figure 4. It is important to note that the progression of growth is similar to Type I in that the oxide ruptures when it reaches some critical layer thickness, h_{fi}. However, when the oxide ruptures in Type II growth, it also detaches from the surface. This results in exposing a larger fresh surface area to the environment, accounting for the wider intrusions characteristically observed with Type II growth.[38] A representative example of each type of growth is shown in Figure 5. Note that the oxide stratifications are visible in Type II; therefore, a direct measure of h_{fi} can be obtained. This is illustrated in Figure 6.

B. *Derivation of the Oxidation Damage Term*

The model is general and is applicable to both Type I and Type II oxide rupture mechanisms. The oxide growth rate is given as

$$\frac{dh_o}{dN} = \frac{dh_o}{dt} \cdot t_c \qquad [5]$$

where t_c is cycle time and dh_o/dN can be considered as an effective oxide growth rate of the primary oxidation-induced crack. The dh_o/dt can be defined by the oxidation kinetics and the critical oxide layer thickness at rupture, h_{fi}. If an oxide layer does not rupture, the model assumes oxidation follows some oxidation growth law. In 1070 steel, oxidation follows parabolic growth,[42] but other oxidation growth laws may be used, depending on the material. The parabolic growth law is $h_o = \sqrt{K_p t}$, where K_p is the parabolic oxidation constant, which is a function of temperature. The time, t, is measured from the instant when fresh metal surface is exposed to the environment.

In general, K_p will not be constant for a cycle which undergoes a varying temperature history. Therefore, an effective oxidation constant, K_p^{eff}, is defined as

$$K_p^{\text{eff}} = \frac{1}{t_c} \int_0^{t_c} D_o \exp\left(\frac{-Q}{RT(t)}\right) dt \qquad [6]$$

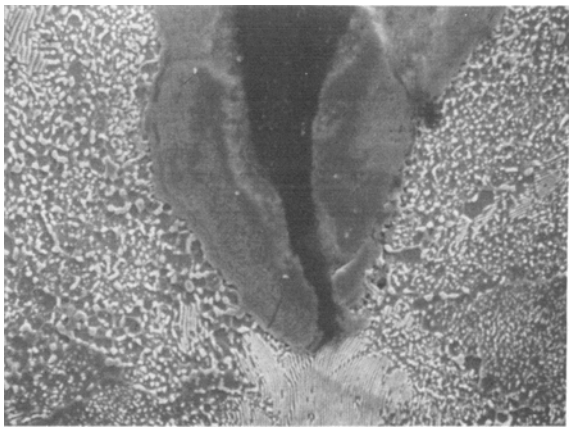

Type I

(*a*)

Loading Direction

10 μm

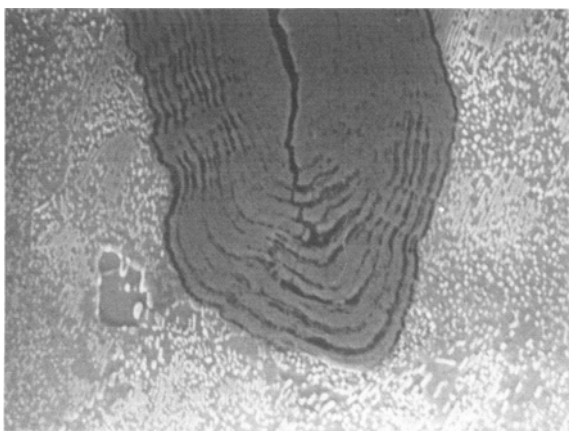

Type II

(*b*)

Fig. 5—SEM micrographs showing oxide intrusion tips resulting from (*a*) Type I growth (out-of-phase TMF, T = 150 °C to 600 °C, $\Delta\varepsilon_{mech}$ = 0.0076, $\dot{\varepsilon} \approx 0.0001\ s^{-1}$) and (*b*) Type II growth (isothermal fatigue, T = 600 °C, $\Delta\varepsilon_{mech}$ = 0.0070, $\dot{\varepsilon}$ = 0.0002 s^{-1}) (5 pct Nital etch).

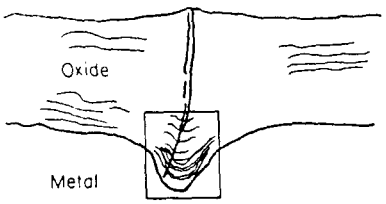

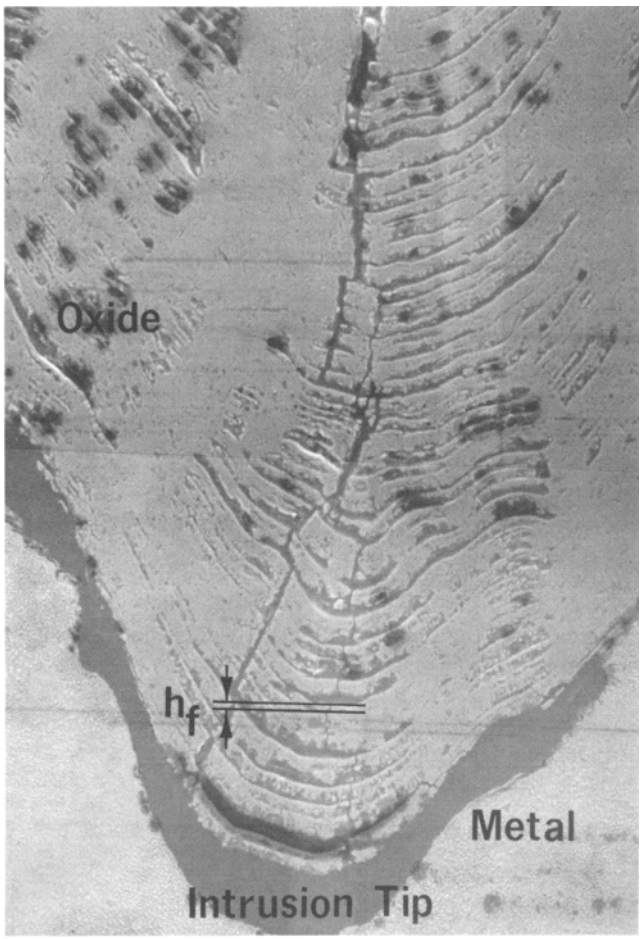

Loading Direction

50 μm

Fig. 6—SEM micrograph illustrating the multilayer oxide and an h_{fi} measurement (out-of-phase TMF, T = 500 °C to 600 °C, $\Delta\varepsilon_{mech}$ = 0.0017, $\dot{\varepsilon} \approx 0.0001\ s^{-1}$).

where D_o is the diffusion coefficient for oxidation, Q is the activation energy for oxidation, R is the universal gas constant, and $T(t)$ is the temperature which can vary with time. Subsequently, K_p^{eff} will be used in the derivation.

If the oxide repeatedly ruptures, then the oxidation growth no longer follows the parabolic law. Upon oxide rupture, a higher localized oxidation rate is observed. This is illustrated in Figure 7 as a series of parabolic curves, with the vertex of the upper parabolic curve located at the point on the one below it where rupture of oxide occurs. Connecting these vertex points creates the effective total oxide growth curve. The slope of this curve gives the effective growth rate, dh_o/dt. The equation of this curve is

$$h_o = B \frac{K_p^{\text{eff}}}{\bar{h}_f} t^{\beta} \qquad [7]$$

where $\bar{h}_f$ is an average value of the critical oxide thickness at rupture and B and β are constants. For the case of linear (*vs* parabolic) oxide growth, $B = \beta = 1$ and $\bar{h}_f = h_{f1}$ = constant, and dh_o/dt = constant. In general, though, the effective growth is nonlinear and will increase with time, as shown in Figure 7, since $h_{fi+1} < h_{fi}$. This occurs due to the increase in the mechanical strain range at the oxide intrusion tip as the intrusion grows. Similarly, increasing the applied mechanical strain range results in decreasing the rupturing thickness of the oxide, h_{fi}, as will be illustrated later.

The growth rate dh_o/dt has been measured in laboratory tests and has a shape similar to the schematic of Figure 8. As shown in Figure 8, the crack length *vs* cycles curves from all three interrupted tests show power law growth (linear on log-log plot) up to a certain crack size.

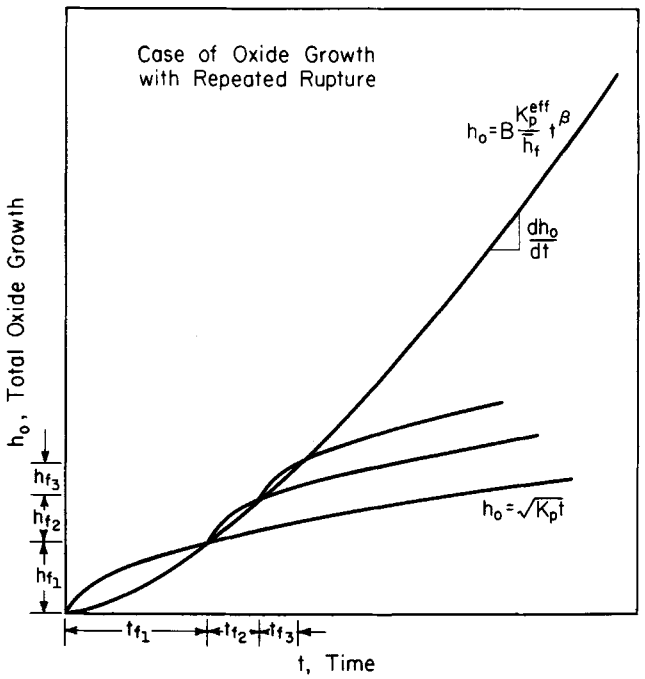

Fig. 7—Diagram illustrating oxide growth with repeated rupture.

Beyond this crack size, rapid crack propagation takes place, and the oxidation effect becomes small. Note that the oxidation-induced crack growth does not operate in the in-phase TMF case. Comparing the in-phase case to out-of-phase TMF and isothermal fatigue, the crack growth rate during the initial portion of life is low. Intergranular damage rapidly accumulates and results in rapid damage in the latter part of life.

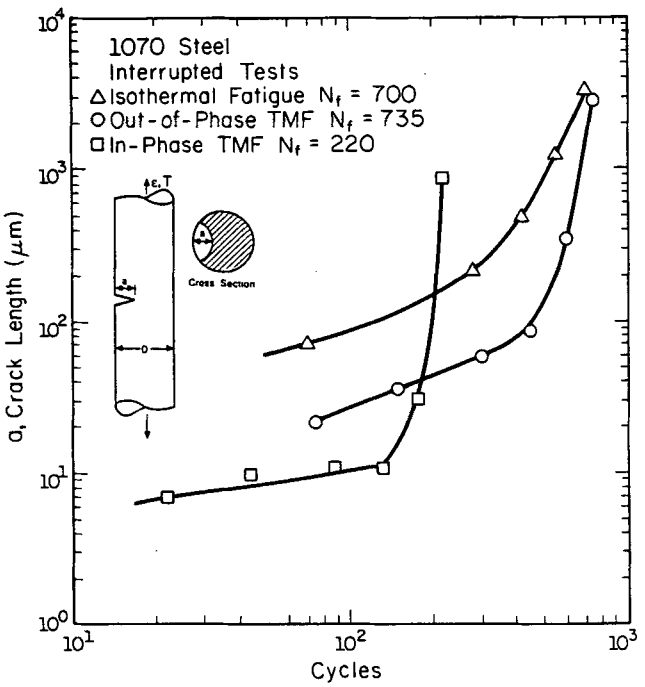

Fig. 8—Crack growth under different strain-temperature phasings ($\Delta\varepsilon_{mech} \approx 0.0076$, $\dot{\varepsilon} \approx 0.0001\ s^{-1}$, T_{min} = 150 °C, T_{max} = 600 °C, T (isothermal) = 600 °C).

Differentiating Eq. [7] with respect to time and substituting this equation back into Eq. [5] gives

$$\frac{dh_o}{dN} = B\frac{K_p^{eff}}{\bar{h}_f}\beta N^{\beta-1}\cdot t_c^{\beta} \qquad [8]$$

The average critical oxide thickness at rupture, $\bar{h}_f$, is a function of the mechanical strain range, the phasing of the temperature and strain, and the strain rate. Experimental measurement of $\bar{h}_f$ (direct measurement of the stratified oxide layer thickness in the oxide intrusions) is plotted against the mechanical strain range, $\Delta\varepsilon_{mech}$, for three different phasing conditions in Figure 9. These results are for the 1070 steel studied here. The experimental results are indicated by data points. The approximate ranges of the data within each phasing are shown in this figure. To quantify the relative damage between phasings, a phasing factor, Φ^{ox}, is introduced. The phasing Φ^{ox} is a function of the ratio of the thermal

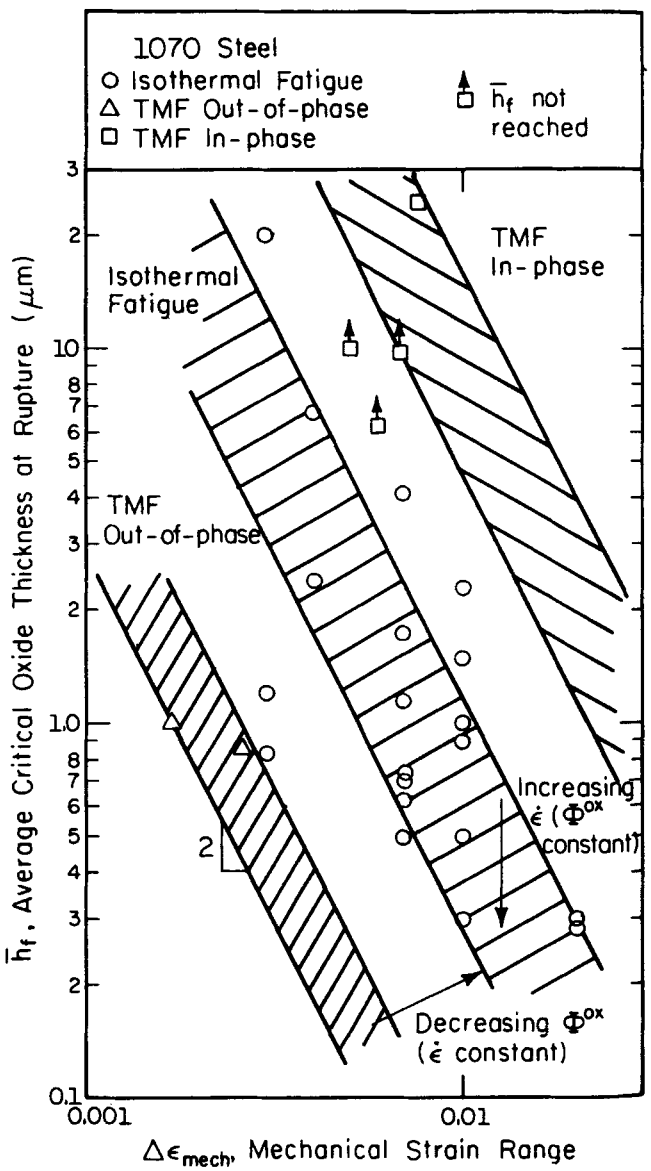

Fig. 9—Plot of average critical oxide thickness at rupture from tests of various phasings.

and mechanical strain rates. It ranges in value from zero, which indicates that no environmental damage results from the phasing, to one, which indicates that the coupling of the environment and phasing is most detrimental to the life. An out-of-phase TMF phasing results in the smallest critical oxide thickness at rupture (Figure 9), and $\Phi^{ox} = 1$. As the phasing changes so that oxide rupture is not as prevalent, Φ^{ox} decreases. Also, as measured from isothermal tests, $\bar{h}_f$ decreased as the strain rate $\dot{\varepsilon}$ increased. Based on these observations shown in Figure 9, curves relating $\Delta\varepsilon_{mech}$, the phasing Φ^{ox}, and the strain rate $\dot{\varepsilon}$ can be expressed by

$$\bar{h}_f = \frac{\delta_o}{(\Delta\varepsilon_{mech})^2 \Phi^{ox} \dot{\varepsilon}^a} \quad [9]$$

where the exponent 2 on $\Delta\varepsilon_{mech}$ represents the slope of the curves in the diagram and δ_o and a are material constants. The constant a predicts the strain rate sensitivity of $\bar{h}_f$; δ_o is a measure of oxide ductility, which is equivalent to $\bar{h}_f$ when $\Delta\varepsilon_{mech}$, Φ^{ox}, and $\dot{\varepsilon}$ are unity, and can be determined from Figure 9.

Substituting Eq. [9] into Eq. [8] and upon integration,

$$\frac{1}{N_f^{ox}} = \left[\frac{h_{cr}\delta_o}{B\Phi^{ox}K_p^{eff}}\right]^{-1/\beta} \frac{2(\Delta\varepsilon_{mech})^{(2/\beta)+1}}{\dot{\varepsilon}^{1-(a/\beta)}} \quad [10]$$

The crack is assumed to grow from zero to some critical length, h_{cr}. Oxide dominated growth ends when $h_o = h_{cr}$, and then crack grows rapidly and oxide penetration trails behind the crack tip. When this occurs, the number of cycles before final failure is very small, and these cycles are neglected in the predictions. Note that the time of a cycle for continuous cycling is written in terms of the mechanical strain range and the strain rate by $t_c = 2\Delta\varepsilon_{mech}/\dot{\varepsilon}$.

C. *Phasing Factor*

Each history is represented by a unique value of Φ^{ox}, defined by integrating ϕ^{ox}, which is a function of the ratio of $\dot{\varepsilon}_{th}/\dot{\varepsilon}_{mech}$, over the period of the history.

$$\Phi^{ox} = \frac{1}{t_c}\int_0^{t_c} \phi^{ox}\, dt \quad [11]$$

The division by t_c allows Φ^{ox} to range from zero to one and thus represents the effective phasing parameter for any strain-temperature history.

The form of ϕ^{ox} was chosen to represent the behavior of the oxide cracking that has been observed experimentally. For example, consider the out-of-phase TMF case: in this case, low temperature and high tensile stresses coincide, and, consequently, the oxide cracks readily. In this case, for a given mechanical strain range, the $\bar{h}_f$ level is small, as shown in Figure 9. If the phasing is represented by the ratio of the thermal and mechanical strain rates, $\dot{\varepsilon}_{th}/\dot{\varepsilon}_{mech} = -1$ represents the out-of-phase TMF case. This case is designated as a benchmark by setting $\phi^{ox} = 1$ at $\dot{\varepsilon}_{th}/\dot{\varepsilon}_{mech} = -1$. For the limiting case of free expansion ($\dot{\varepsilon}_{th}/\dot{\varepsilon}_{mech} \rightarrow \pm\infty$), ϕ^{ox} should approach zero. Other histories designated by $\dot{\varepsilon}_{th}/\dot{\varepsilon}_{mech}$ will have unique values of ϕ^{ox}, which fall between the limits of zero and one. The level of $\bar{h}_f$ at a given strain range is higher in the in-phase TMF case ($\dot{\varepsilon}_{th}/\dot{\varepsilon}_{mech} = 1$) compared to the isothermal fatigue case ($\dot{\varepsilon}_{th}/\dot{\varepsilon}_{mech} = 0$), as indicated in Figure 9.

Based on these observations, the function ϕ^{ox} was chosen to be

$$\phi^{ox} = \exp\left[-\frac{1}{2}\left(\frac{(\dot{\varepsilon}_{th}/\dot{\varepsilon}_{mech}) + 1}{\xi^{ox}}\right)^2\right] \quad [12]$$

The parameter ξ^{ox} is introduced as a measure of the relative amount of damage associated with the different phasings. This exponential function is plotted in Figure 10 for several ξ^{ox} values. In this case, the curves show that peak damage occurs when $\dot{\varepsilon}_{th}/\dot{\varepsilon}_{mech} = -1$ (out-of-phase TMF, total constraint).

D. *Determination of the Oxidation Damage Term Constants*

In this section, it is shown how each constant in the oxidation damage term is established.

ξ^{ox}: Consider two tests which have different strain-temperature phasings, and N_f^{ox} dominates the damage sum. One of these tests is an out-of-phase TMF, since ϕ^{ox} is assumed to be one for this case. The $\dot{\varepsilon}$, $\Delta\varepsilon_{mech}$, and K_p^{eff} should be approximately the same for both cases. N_f^{ox} is known for both cases. Therefore, only ϕ_2^{ox} (subscripts distinguish between the two tests) for the second test is unknown and can be solved for by rearranging Eq. [10].

$$\phi_2^{ox} = \phi_1^{ox}\left(\frac{N_{f1}^{ox}}{N_{f2}^{ox}}\right)^{\beta}\left(\frac{K_{p1}^{eff}}{K_{p2}^{eff}}\right)\left(\frac{\dot{\varepsilon}_2}{\dot{\varepsilon}_1}\right)^{\beta-a}\left(\frac{\Delta\varepsilon_{mech\,1}}{\Delta\varepsilon_{mech\,2}}\right)^{2+\beta} \quad [13]$$

By substituting this value of ϕ_2^{ox} into Eq. [12], ξ^{ox} can be determined. The two tests used were

(1) out-of-phase TMF, $T = 150$ °C to 600 °C, $\Delta\varepsilon_{mech\,1} = 0.0076$, $\dot{\varepsilon}_1 \approx 0.0001\ s^{-1}$, $N_{f1}^{ox} \approx 7.35$, $\phi_1^{ox} = 1$; and

(2) isothermal fatigue, $T = 600$ °C, $\Delta\varepsilon_{mech\,2} = 0.0070$, $\dot{\varepsilon}_2 = 0.0002\ s^{-1}$, $N_{f2}^{ox} \approx 700$.

Based on the above analysis, $\phi_2^{ox} = 0.88$ and $\xi^{ox} \approx 2$. The function ϕ^{ox} using this value has been shown in Figure 10.

a: Consider two isothermal fatigue experiments at strain rates $\dot{\varepsilon}_1 = 0.0002\ s^{-1}$ and $\dot{\varepsilon}_2 = 0.02\ s^{-1}$. From Figure 9,

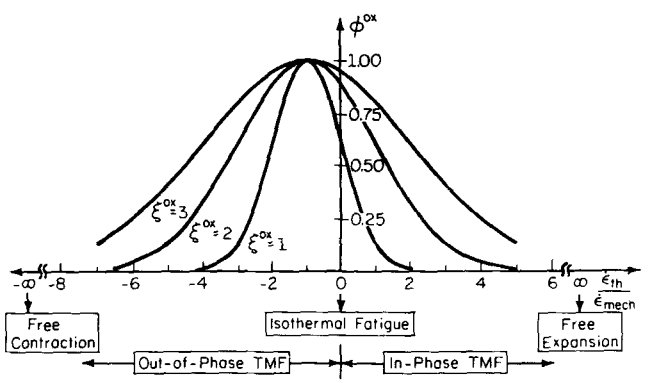

Fig. 10—Plot showing the ϕ^{ox} function for three different ξ^{ox} values with peak damage occurring at $\dot{\varepsilon}_{th}/\dot{\varepsilon}_{mech} = -1$.

one can determine from the isothermal case the corresponding $\bar{h}_f$ values for both of these strain rates at a constant $\Delta\varepsilon_{mech}$. It is assumed that the strain rate sensitivity of $\bar{h}_f$ under isothermal conditions is the same as under thermal cycling conditions. Then,

$$a = \frac{\ln\left(\frac{\bar{h}_{f1}}{\bar{h}_{f2}}\right)}{\ln\left(\frac{\dot{\varepsilon}_2}{\dot{\varepsilon}_1}\right)} \qquad [14]$$

δ_o: This material constant represents the value of the $\bar{h}_f$-axis intercept at $\Delta\varepsilon_{mech} = 1$, when Φ^{ox} and $\dot{\varepsilon}$ are also unity. One laboratory test which has a multilayered oxide (Type II growth behavior) is required to obtain the following constant:

isothermal fatigue, $T = 600$ °C, $\Delta\varepsilon_{mech} = 0.01$, $\dot{\varepsilon} = 0.0002\ s^{-1}$, $\bar{h}_f \approx 1.5\ \mu m$, $\Phi^{ox} = 0.88$.

By solving for δ_o in Eq. [9],

$$\delta_o = \bar{h}_f(\Delta\varepsilon_{mech})^2\Phi^{ox}\dot{\varepsilon}^a \qquad [15]$$

and substituting the above test parameters, the constant, δ_o, was determined. In this study, δ_o was found to be $2.22 \times 10^{-7}\ \mu m \cdot s^{-0.75}$. The value of $\bar{h}_f$ is the average value of h_{fi} measured from micrographs, such as shown in Figure 6.

D_o and Q: D_o is the diffusion coefficient, and Q is the activation energy for oxidation. They were established from oxide growth measurements on specimens subjected to zero load. Two temperatures were considered to obtain the constants: 600 °C and 400 °C. The parabolic growth constant, K_p, was determined at both of these temperatures by fitting a parabolic curve through the experimental data. Since

$$K_p = D_o e^{(-Q/RT)} \qquad [16]$$

D_o and Q can be calculated. In Figure 11, the growth curves for various temperatures, as established from Eq. [16], are plotted along with the laboratory data used to obtain the constants.

β: This constant is the exponent on t for the effective oxidation-induced growth curve (Figure 7). It was chosen to represent the crack growth behavior observed in laboratory tests (Figure 8). Experimental results indicate an average value of $\beta = 1.5$.

B, h_{cr}: These two constants are interrelated. The units on B are $(s^{1-\beta})$ (Eq. [7]), and the units on h_{cr} are (μm). Consider a test which is used to obtain the critical crack length, h_{cr}. There is a corresponding time to reach this length, and B is related to this time. Using life and cycle time from this test, the constant B is obtained by

$$B = (t_c \cdot N_f^{ox})^{1-\beta} \qquad [17]$$

In this study, the following test was used:

isothermal fatigue, $T = 600$ °C, $\Delta\varepsilon_{mech} = 0.01$, $\dot{\varepsilon} = 0.0002\ s^{-1}$, $N_f = 228$.

The value of h_{cr} was determined from Eq. [10], where N_f^{ox}, the test parameters $(\Delta\varepsilon_{mech}, \dot{\varepsilon})$, and other constants for the same experiment used to compute B are known.

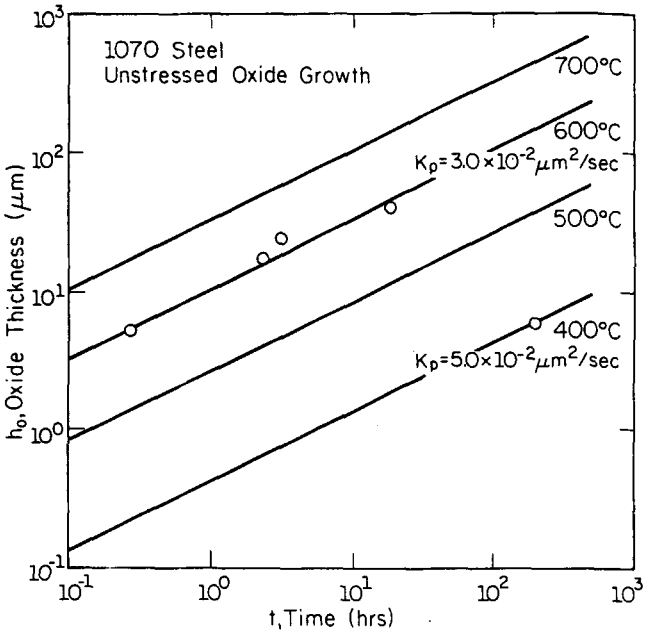

Fig. 11—Plot of the unstressed parabolic growth at various temperatures.

IV. CREEP DAMAGE TERM

A. *Measure of Creep Damage*

Most creep damage, which is detectable with the scanning electron microscope (SEM), is in the form of internal intergranular cracking (*e.g.*, Figure 12). This damage was only observed in the in-phase TMF test specimens. None of the isothermal (20 °C to 700 °C) or out-of-phase TMF tests had any detectable intergranular damage.

The in-phase TMF 150 °C to 600 °C test was one of the tests considered in the interrupted study. It was found that below 60 pct N_f, no creep damage in the form of intergranular cracking (greater than 0.10 μm) was observed. At 60 pct N_f, a few small (less than 1.0 μm) cavities along grain boundaries were detected. Significant measurable damage was not found until 100 pct N_f was reached.

The growth of voids and intergranular crack growth occur predominantly under tensile loading.[34,43] Consequently, to take into account the asymmetry, the creep damage term is a function of effective and hydrostatic stress components

$$D^{creep} = \Phi^{creep} \int_0^{t_c} A e^{(-\Delta H/RT)} \left(\frac{\alpha_1\bar{\sigma} + \alpha_2\sigma_H}{K}\right)^m dt \qquad [18]$$

where $\bar{\sigma}$ is the effective stress, σ_H is the hydrostatic stress, K is the drag stress, α_1 and α_2 are scaling factors which represent the relative amount of damage occurring in tension and compression, Φ^{creep} is the phasing factor, and A and m are material constants. In order to use this equation, a constitutive model must be employed which can relate the inelastic strain rates to the stresses. This is necessary to handle different strain rates, thermomechanical loadings, and hold-time effects.

For the predictions in this report, a unified constitutive

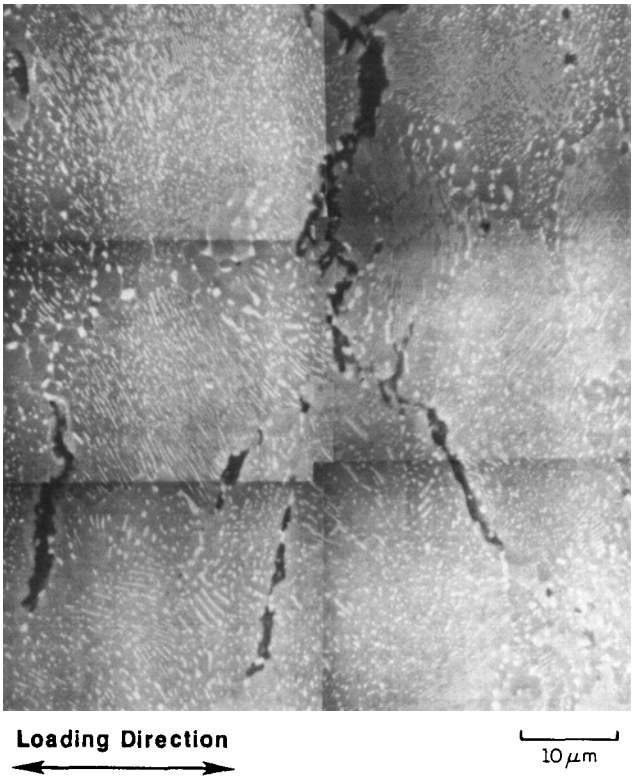

Fig. 12—SEM micrograph showing intergranular cracking from in-phase TMF cycling with T = 150 °C to 600 °C (5 pct Nital etch).

model recently developed for 1070 steel[44,45] is used. This model utilizes two state variables, as follows: (1) the drag stress K, which is a measure of strength, and (2) back stress α, which is recognized as an internal stress, reflecting the nonisotropy in the material. In creep, the back stress α accounts for nonisotropy as well as transient creep behavior. Since it is desirable to obtain the creep damage for the stable cycle, a simplification is made in the constitutive model so that the approximate stable response can be directly obtained, bypassing any initial transient behavior. This is accomplished by setting the drag stress to the saturated value, $K = K_{sat}$, where K_{sat} is a function of the temperature, and setting the back stress to zero, $\alpha = 0$.

For all in-phase TMF tests, including the lowest temperature range test performed (150 °C to 450 °C), internal intergranular cracking is observed, which results from the growth of voids and subsequent intergranular creep damage. In all isothermal test specimens (fully reversed loading and symmetric wave form), no intergranular damage is observed, and all cracking is transgranular. This indicates that different damage mechanisms are operating in each of these tests, and this must be reflected in the creep damage equation.

A phasing factor, Φ^{creep}, similar to the one used in the oxidation damage term, is incorporated into the creep damage term. The phasing factor for creep will have the same form (Eqs. [11] and [12]) as the Φ^{ox} factor for oxidation. For example,

$$\Phi^{creep} = \frac{1}{t_c}\int_0^{t_c} \phi^{creep}\, dt \qquad [19]$$

where ϕ^{creep} is an exponential function of $\dot{\varepsilon}_{th}/\dot{\varepsilon}_{mech}$, characterizing the severity of the creep damage for any ratio of the thermal and mechanical strain rates. This function is represented by a normal distribution for which the peak ($\phi^{creep} = 1$) occurs, where the phasing of the thermal and mechanical strain rates is most damaging:

$$\phi^{creep} = \exp\left[-\frac{1}{2}\left(\frac{(\dot{\varepsilon}_{th}/\dot{\varepsilon}_{mech}) - 1}{\xi^{creep}}\right)^2\right] \qquad [20]$$

The constant, ξ^{creep}, defines the sensitivity of the phasing to the creep damage. This function is shown plotted in Figure 13. From laboratory tests, the in-phase TMF case ($\dot{\varepsilon}_{th}/\dot{\varepsilon}_{mech} = 1$) shows the most creep damage (creep voids and intergranular cracking); therefore, this case is assigned the value $\phi^{creep} = 1$, as shown in Figure 13. By comparing the N_f^{creep} experimental values for two different phasings, an assessment of the sensitivity to the phasing, and thus ξ^{creep}, can be obtained. Based on an isothermal fatigue and in-phase TMF test, $\xi^{creep} \approx 0.40$. The distribution of ϕ^{creep} shown in Figure 13 incorporates this value.

B. *Determination of the Creep Damage Term Constants*

α_1, α_2: First, α_1 and α_2 are determined. These constants are included in the model because of the recognition that the microstructural creep damage in tension differs from compression. If it is assumed that no creep damage accumulates in compression (as assumed in 1070 steel), $\alpha_1 = 1/3$, and $\alpha_2 = 1$ for uniaxial loading.

ΔH: The activation energy for creep, ΔH, is experimentally determined from creep tests. The value of ΔH is 248.1 kJ/mol for 1070 steel.[46]

A, m: These constants are interrelated and must be determined in a systematic fashion. By substituting two laboratory test results each into Eq. [18], two equations and two unknown constants can be obtained. However, Eq. [18] requires that the experimental value for N_f^{creep} be used. The following can be estimated by rearranging Eq. [2] and using the experimental life N_f^{exp}, instead of N_f:

$$\frac{1}{N_f^{creep}} = \frac{1}{N_f^{exp}} - \frac{1}{N_f^{fat}} - \frac{1}{N_f^{ox}} \qquad [21]$$

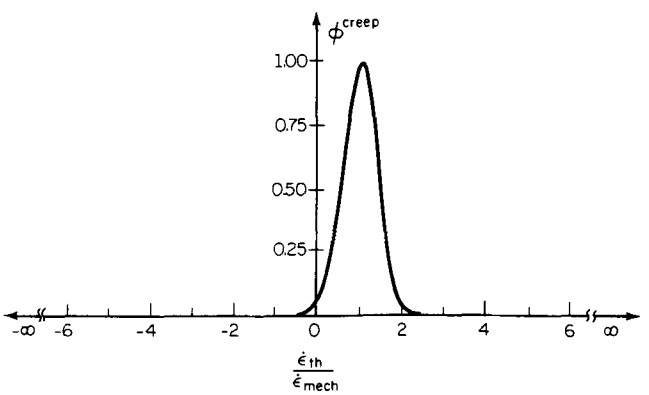

Fig. 13—Plot of the creep phasing function, ϕ^{creep}.

The following two tests were used to obtain the following constants:

(1) isothermal fatigue, helium, T = 600 °C, $\Delta\varepsilon_{mech}$ = 0.0030, $\dot{\varepsilon}$ = 0.0002 s^{-1}, N_f^{exp} = 60,914, N_f^{fat} = 440,683.

(2) isothermal fatigue, helium, T = 600 °C, $\Delta\varepsilon_{mech}$ = 0.0030, $\dot{\varepsilon}$ = 0.02 s^{-1}, N_f^{exp} = 250,000, N_f^{fat} = 440,683.

By using helium tests, the last term of Eq. [21] is eliminated ($1/N_f^{ox} \rightarrow 0$). The N_f^{fat} contribution is determined from the strain-life equation (Eq. [3]).

The life of the lower strain rate helium test is much less than the high strain rate test, indicating that nonenvironmental time-dependent mechanisms must be producing damage. Therefore, it is valid to use these two tests to estimate the creep damage constants A and m.

V. RESULTS

The predictions for many testing conditions are plotted as strain-life curves in Figures 14 through 22. A list of all the constants used in the prediction model is provided in Table I. Included on the prediction plots are 1070 steel life data. Some of the data have been reported elsewhere.[38,47] Twelve tests were used to establish the constants, and a total of 86 tests were predicted.

Predictions of isothermal fatigue tests performed at 600 °C in air are given in Figure 14. The lines on this plot indicate the prediction curves at three strain rates used in the testing program. Test data are indicated by symbols. The governing damage mechanism is oxidation for all cases except the $\dot{\varepsilon}$ = 0.02 tests at $\Delta\varepsilon$ = 0.007 and 0.01. The model correctly predicts that there is little time available for the oxidation damage mechanism to operate in these two test cases.

Predictions and laboratory tests for comparable out-of-phase and in-phase TMF tests are shown on Figures 15 and 16. For both phasings, T_{min} = 150 °C. When $\Delta\varepsilon_{mech}$ is small (which corresponds to a maximum temperature less than 500 °C), the governing damage mechanism is fatigue. As $\Delta\varepsilon_{mech}$ increases (with the corresponding increase in temperature), the mechanism changes to oxidation for out-of-phase TMF and to creep for in-phase TMF. In the case of out-of-phase loading, the oxide experiences tension at the low-temperature end of the cycle, while in the case of in-phase loading, the specimen is in tension at the high-temperature end, resulting in the operation of the void growth and intergranular cracking mechanisms.

Additional isothermal fatigue predictions are given in Figures 17 and 18 for temperatures 20 °C and 400 °C. The prediction for 20 °C (Figure 17) degenerates into the strain-life curve given by Eq. [3], because neither oxidation nor creep mechanisms operate. At 400 °C (Figure 18), only small mechanical strain ranges show any strain rate dependence on the life. At temperatures below 400 °C, the isothermal predictions resemble the 20 °C strain-life curve. Isothermal predictions at 600 °C show a strain rate dependence on life, as was shown previously in Figure 14.

Predictions and experimental test data for other total constraint out-of-phase TMF tests with T_{min} different from

Table I. Material Constants for 1070 Steel

Material Constants Used in Fatigue Strain-Life Term (20 °C)	
E	= 200,860 MPa
σ_f'	= 958.0 MPa
b	= −0.093
ε_f'	= 0.0996
c	= −0.464
Material Constants Used in Oxidation Damage Term	
a	= 0.75
β	= 1.5
B	= 6.62×10^{-3} $s^{-0.5}$
δ_o	= 2.22×10^{-7} $\mu m \cdot s^{-0.75}$
D_o	= 6.95×10^{7} $\mu m^2/s$
Q	= 156.5 kJ/mol
h_{cr}	= 458.0 μm
ξ^{ox}	= 2.0
Material Constants Used in Creep Damage Term	
A	= 1.562×10^{14} s^{-1}
m	= 11.34
ΔH	= 248.1 kJ/mol
ξ^{creep}	= 0.40
Simple Constitutive Law to Predict Stresses[44]	
$\dot{\bar{\varepsilon}}^{in}$	= $A_c \exp[-\Delta H_c/R(T + 273)] f(\bar{\sigma}/K)$
A_c	= 4.0×10^{9} s^{-1}
ΔH_c	= 210.6 kJ/mol

$$f(\bar{\sigma}/K) = \begin{cases} (\bar{\sigma}/K)^{5.4} & \bar{\sigma}/K < 1.0 \\ \exp[(\bar{\sigma}/K)^{8.3} - 1.0] & \bar{\sigma}/K > 1.0 \end{cases}$$

$K = K_{sat}$ (in this study)

$$K_{sat} = \begin{cases} 256.0 + 1.4 \times 10^{-3} T^2 & T < 304\ ^\circ C \\ 568.0 - 0.6\,T & T > 304\ ^\circ C \end{cases} \text{(MPa)}$$

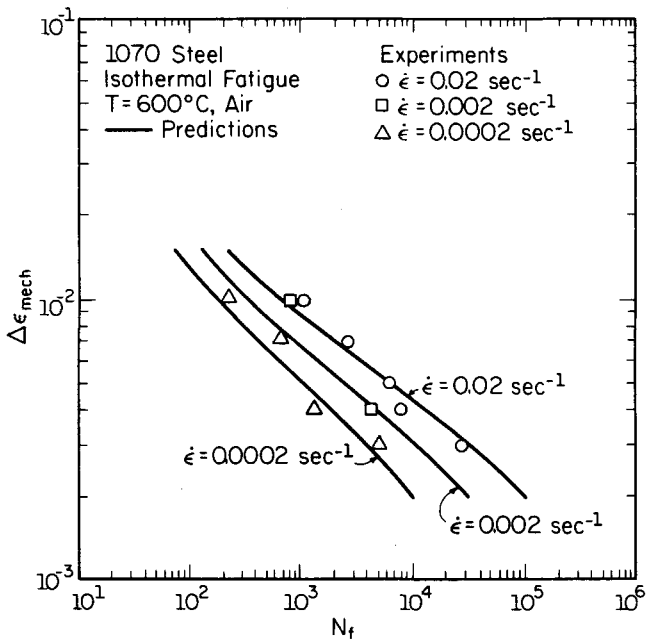

Fig. 14 — Comparison of predicted and experimental lives in air for isothermal fatigue with T = 600 °C.

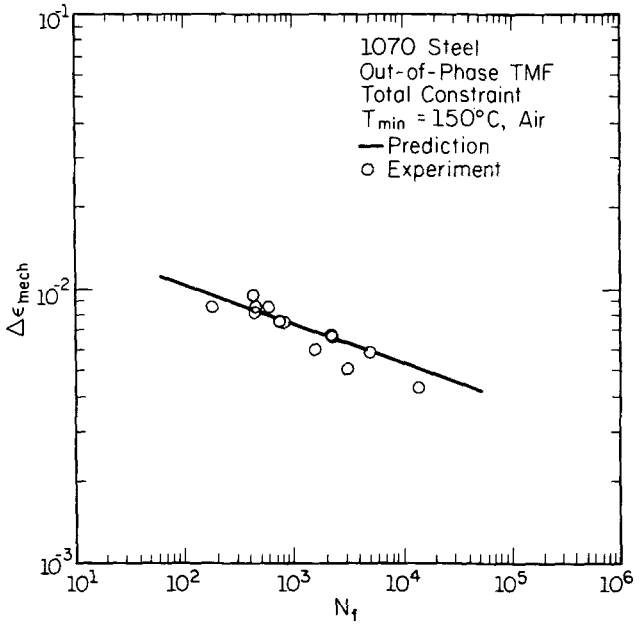

Fig. 15—Comparison of predicted and experimental lives in air for out-of-phase total constraint TMF with T_{min} = 150 °C.

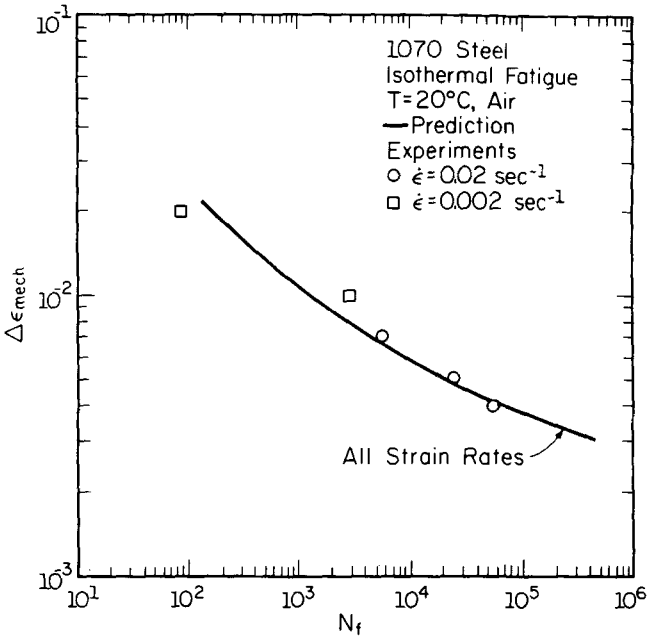

Fig. 17—Comparison of predicted and experimental lives in air for isothermal fatigue with T = 20 °C.

150 °C are shown in Figure 19. These confirm that the model works for any general temperature range.

One advantage of this prediction model is its ability to handle tests of any given phasing. Two additional phasings, for which experimental data are available, are partial constraint and over contraint out-of-phase TMF (Figure 1). For partial constraint, $\dot{\varepsilon}_{th}/\dot{\varepsilon}_{mech} < -1$. The prediction for the experimental tests performed at $\dot{\varepsilon}_{th}/\dot{\varepsilon}_{mech} \approx -2$ is given in Figure 20. When $\dot{\varepsilon}_{th}/\dot{\varepsilon}_{mech}$ is between 1 (total constraint, $\Delta\varepsilon_{mech} = \Delta\varepsilon_{th}$) and 0 (isothermal conditions), over constraint conditions exist. The prediction for the case $\Delta\varepsilon_{mech} = 2\Delta\varepsilon_{th}$ ($\dot{\varepsilon}_{th}/\dot{\varepsilon}_{mech} = -0.5$) is also included in Figure 20. Reasonably good predictions are demonstrated.

Tests in helium are also considered. Isothermal helium tests were performed at 600 °C, and out-of-phase and in-phase TMF helium tests were performed with T_{min} = 150 °C. The predictions and laboratory test data are shown in Figures 21 and 22. For isothermal fatigue (Figure 21), the slowest strain rate is predicted to be less damaging than the intermediate strain rate, contrary to all tests performed on this material. Since D^{ox} = zero and D^{fat} = constant at all three strain rates, the problem lies entirely

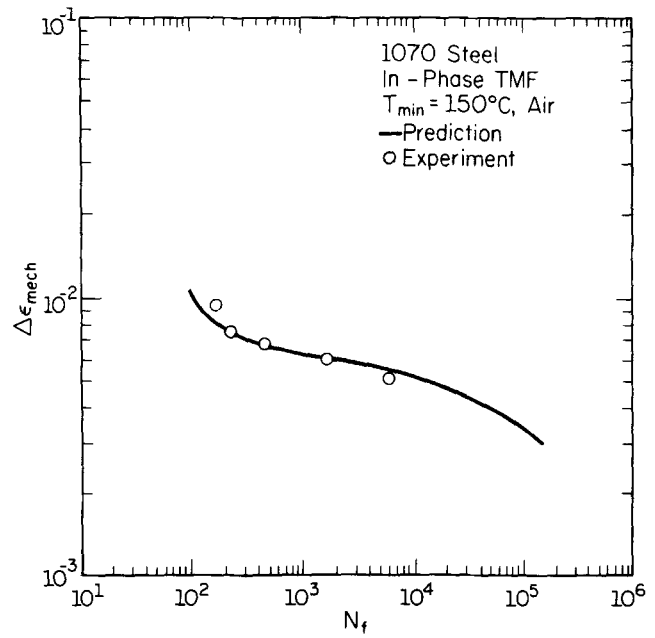

Fig. 16—Comparison of predicted and experimental lives in air for in-phase TMF with T_{min} = 150 °C.

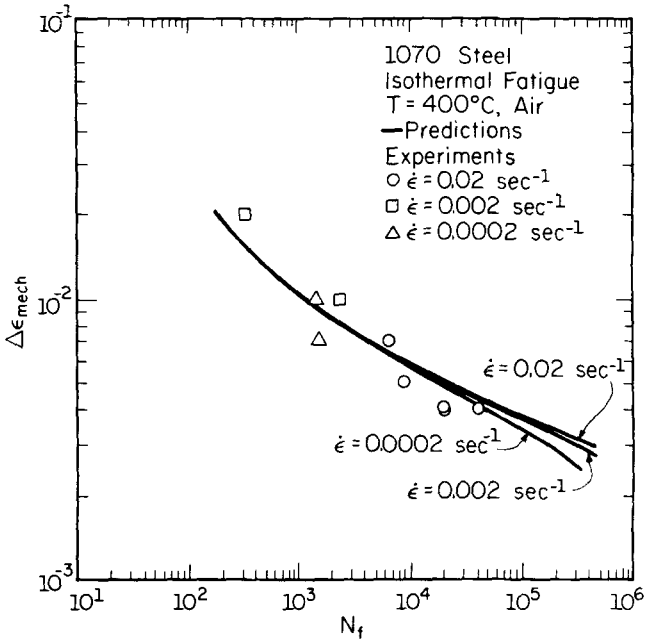

Fig. 18—Comparison of predicted and experimental lives in air for isothermal fatigue with T = 400 °C.

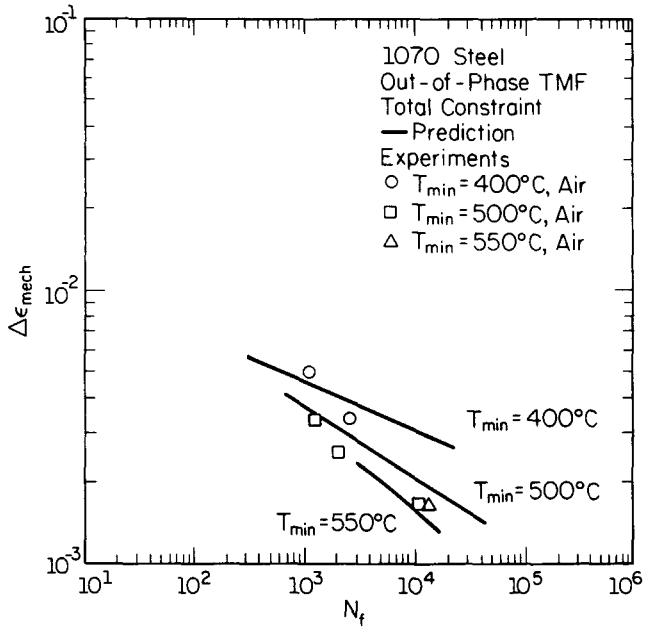

Fig. 19—Comparison of predicted and experimental lives in air for out-of-phase total constraint TMF ($\dot{\epsilon}_{th}/\dot{\epsilon}_{mech} = -1$) with T_{min} = 400 °C, T_{min} = 500 °C, and T_{min} = 550 °C.

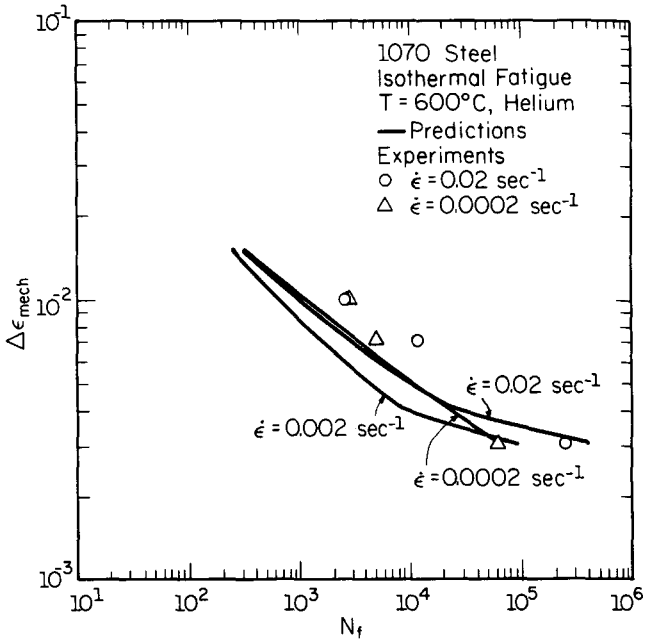

Fig. 21—Comparison of predicted and experimental lives in helium for isothermal fatigue with T = 600 °C.

in the computation of D^{creep}. The flow rule relates the effective inelastic strain rate to the effective stress $\bar{\sigma}$ normalized with the drag stress K.[44,45] As the applied strain rate is decreased, $\bar{\sigma}/K$ decreases, and the flow rule changes from an exponential function to a power law function (Table I). This results in a much greater decrease in stress with decrease in strain rate at 600 °C, and damage decreases more rapidly.

In addition, the predictions of isothermal helium tests indicate that as the mechanical strain range is increased, the strain rate dependence decreases. The tests are shorter, and, thus, creep damage is minimal. The laboratory tests performed at the largest $\Delta\varepsilon_{mech}$ have nearly identical lives, confirming the trend observed in the prediction.

Out-of-phase and in-phase TMF helium tests were predicted, and the results are shown in Figure 22. Note that the prediction for the out-of-phase tests degenerates

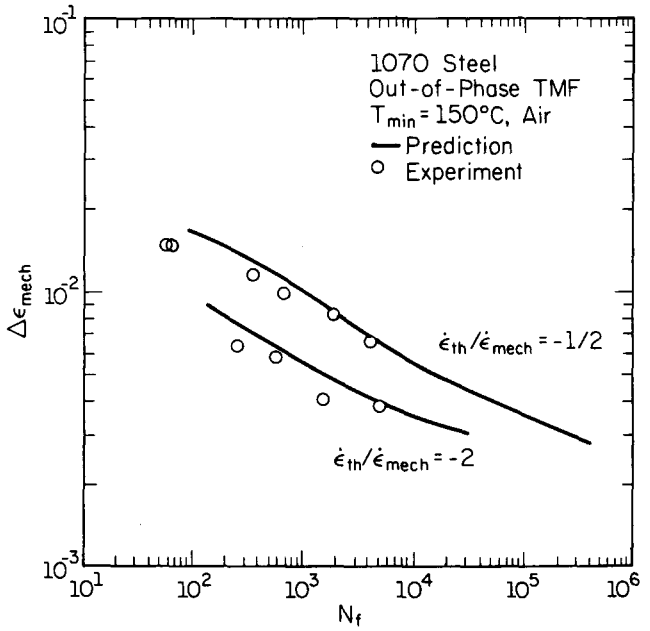

Fig. 20—Comparison of predicted and experimental lives in air for out-of-phase partial constraint TMF ($\dot{\epsilon}_{th}/\dot{\epsilon}_{mech} = -2$), T_{min} = 150 °C, and out-of-phase over constraint TMF ($\dot{\epsilon}_{th}/\dot{\epsilon}_{mech} = -0.5$), T_{min} = 150 °C.

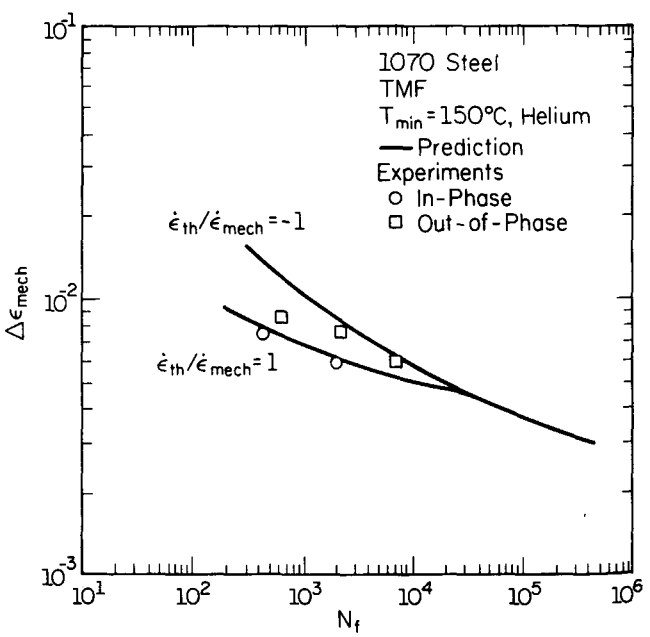

Fig. 22—Comparison of predicted and experimental lives in helium for out-of-phase ($\dot{\epsilon}_{th}/\dot{\epsilon}_{mech} = -1$) and in-phase ($\dot{\epsilon}_{th}/\dot{\epsilon}_{mech} = 1$) TMF with T_{min} = 150 °C.

into the fatigue strain-life curve. For this phasing, $N_f^{creep} \approx 0$, and because the tests were performed in helium, $N_f^{ox} = 0$.

VI. DISCUSSION

The advantages of this life prediction model are the following: (a) it can handle any arbitrary strain-temperature phasing (in-phase and out-of-phase TMF and others); (b) it works for a wide range of temperatures (20 °C to 650 °C), strain rates ($\dot{\varepsilon} = 0.02$ to $0.0002\ s^{-1}$), mechanical strain ranges ($\Delta\varepsilon_{mech} = 0.0030$ to 0.0200), and atmospheres (air or inert); (c) the constants are directly linked to experiments; (d) the oxide rupture is accounted for by the temperature, strain rate, and strain dependence; (e) the creep term is stress-based and has the capacity for treating compressive stresses as damaging or nondamaging; and (f) the creep term is also coupled with a unified constitutive equation that predicts the stresses for a given history.

The fatigue, oxidation, and creep damage terms are derived independently. Thus, the damage mechanism which is the most dominant is determined readily. Oxidation and creep damage terms reported are based on physical damage mechanisms. Both these damage terms represent a dependence on temperature and the thermal strain rate/mechanical strain rate ratio. Therefore, a change in either of these parameters would affect both damage terms. Direct coupling of fatigue with either oxidation or creep is considered to be a second-order effect for this material. Other investigations[8] reached a similar conclusion for other materials. Direct coupling effects between oxidation and fatigue terms could be investigated by performing high strain rate tests that are initiated in air, in which both oxidation and fatigue mechanisms operate, and then continued in helium, in which fatigue alone operates. The high strain rate eliminates creep damage, so that crack nucleation occurs by the oxidation-induced process and its effect on subsequent crack growth in the absence of oxidation will result.

The model is not limited to continuous symmetric wave shape cycling. The oxidation and creep equations (Eqs. [10] and [18]) may be integrated to obtain expressions for other complex wave shapes, including hold-time effects. However, any hold time in isothermal fatigue does not tend to oxidation damage. This is explained by the initial assumption for the oxidation damage model that oxidation-induced growth occurs by a rupturing process in this material. Under a strain or stress hold, the oxide is assumed not to rupture. Furthermore, since no rupturing of the oxide occurs under a hold time, the environmental attack will lessen with time, because oxidation kinetics predict a decreasing oxidation rate from the parabolic law, as the oxide grows thicker if no rupturing occurs. If the material developed an oxide which fractured with no aid from strain cycling, hold time would be readily incorporated into the oxidation damage term. Nevertheless, the overall model will predict that the effect of hold times is damaging when creep damage is present. For example, under strain holds when stress relaxation occurs, the creep damage term evolves with time.

Considering the broad range of testing parameters examined, the predictions are quite satisfactory. Eighty-four percent of the predictions are within a factor ±2.5 of the experimental life. Moreover, for many of the TMF tests, the scatter in the experimental lives affects the appearance of the accuracy of the model.

VII. SUMMARY

A comprehensive life prediction model, which is based on the sum of the fatigue, oxidation, and creep damage components, is proposed. A method to predict the effects of arbitrary strain-temperature phasings on the oxidation and creep damage is proposed. The model is applied to 1070 steel in this paper, and it shows promise for predicting fatigue lives for other alloys, including a Ni-based superalloy.[48]

The fatigue damage is based on the strain-life equation[37] with constants determined at room temperature. This damage expression gives an upper bound on life.

The oxidation damage is based on a repeated microrupture of the oxide at the oxide "intrusion" tip. This rupture process is a function of mechanical strain range, strain rate, strain-temperature phasing, and oxidation kinetics.

The creep damage is based on stress, temperature, strain-temperature phasing, and time. The stress history is determined using a unified constitutive equation.

NOMENCLATURE

A	coefficient in creep damage equation
A_c	flow rule coefficient in constitutive law
a	strain rate sensitivity constant in oxidation term
B	coefficient in oxidation growth equation
b	fatigue strength exponent
c	fatigue ductility exponent
D_o	diffusion coefficient for oxidation
D^{creep}	creep damage per cycle
D^{fat}	fatigue damage per cycle
D^{ox}	oxidation damage per cycle
D^{tot}	total damage per cycle
E	Young's modulus
h_{cr}	critical total oxide growth when oxidation-induced crack growth ends and rapid crack growth begins
h_{fi}	critical oxide layer thickness at fracture
h_f	average value of the critical oxide layer thickness at fracture
h_o	total oxide growth
K	drag stress
K_p	parabolic oxidation constant
K_p^{eff}	effective parabolic oxidation constant
K_{sat}	saturated drag stress
m	exponent on stress in creep damage equation
N	number of cycles
N_f	number of cycles to specimen failure
N_f^{creep}	number of cycles to failure from creep damage
N_f^{exp}	number of cycles to failure from experimental tests

N_f^{fat}	number of cycles to failure from fatigue damage
N_f^{ox}	number of cycles to failure from oxidation damage
N_f^P	long crack propagation life (cycles)
N_f^{tot}	total number of cycles of a component
Q	activation energy for oxidation
R	universal gas constant
T	temperature
T_{max}	maximum temperature of a TMF cycle
T_{min}	minimum temperature of a TMF cycle
t	time
t_c	period of a cycle
α	back stress
α_1, α_2	constants which represent the asymmetry of creep damage
β	exponent on time in oxidation growth equation
$\Delta\varepsilon_{mech}$	mechanical strain range
ΔH	activation energy for the rate-controlling creep mechanism
ΔH_c	activation energy in constitutive law
δ_o	measure of oxide ductility (material constant)
ε_{mech}	mechanical strain
ε_{th}	thermal strain
ε_f'	fatigue ductility coefficient
$\dot{\bar{\varepsilon}}^{in}$	equivalent inelastic strain rate
$\dot{\varepsilon}$, $\dot{\varepsilon}_{mech}$	mechanical strain rate
$\dot{\varepsilon}_{th}$	thermal strain rate
Φ^{creep}	phasing factor for creep
Φ^{ox}	phasing factor for oxidation
ϕ^{creep}	phasing function for creep
ϕ^{ox}	phasing function for oxidation
σ_H	hydrostatic stress
$\bar{\sigma}$	effective stress
σ_f'	fatigue strength coefficient
ξ^{creep}	shape factor for creep phasing function
ξ^{ox}	shape factor for oxidation phasing function

ACKNOWLEDGMENTS

This work was supported by the Association of American Railroads, Technical Center, Chicago, IL. The cooperation of Dr. Daniel Stone, Director of Metallurgy, and Mr. Michael Fec, Senior Engineer, is appreciated.

REFERENCES

1. R.S. Nelson, J.F. Schoendorf, and L.S. Lin: *Creep Fatigue Life Prediction for Engine Hot Section Materials (Isotropic)-Interim Report*, NASA CR-179550, Dec. 1986.
2. L.F. Coffin, Jr.: *Fatigue at Elevated Temperatures*, ASTM STP 520, 1973, pp. 5-34.
3. K.D. Challenger, A.K. Miller, and R.L. Langdon: *J. Materials for Energy Systems*, 1981, vol. 3 (6), pp. 51-61.
4. S.D. Antolovich, R. Baur, and S. Liu: *Superalloys 1980*, 1980, pp. 605-13.
5. S.D. Antolovich, S. Liu, and R. Baur: *Metall. Trans. A*, 1981, vol. 12A, pp. 473-81.
6. J. Reuchet and L. Rémy: *Metall. Trans. A*, 1983, vol. 14A, pp. 141-49.
7. R.P. Skelton and J.I. Bucklow: *Met. Sci.*, 1978, vol. 12 (2), pp. 64-70.
8. A. Saxena and J.L. Bassani: *Proc. AIME on Fracture: Interactions of Microstructure, Mechanisms, and Mechanics*, J.M. Wells and J.D. Landes, eds., 1984, pp. 357-83.
9. H.W. Liu and Y. Oshida: *Theoretical and Applied Fracture Mechanics*, 1986, vol. 6, pp. 85-94.
10. L.F. Coffin, Jr.: *Metall. Trans.*, 1972, vol. 3, pp. 1777-88.
11. R. Skelton: *Mater. Sci. and Eng.*, 1978, vol. 35 (2), pp. 287-98.
12. S. Floreen and R.H. Kane: *Fatigue of Engineering Materials and Structures*, 1980, vol. 2, pp. 401-12.
13. R.P. Skelton: *Low-Cycle Fatigue and Life Prediction*, ASTM STP 770, 1982, pp. 337-81.
14. E. Renner, H. Vehoff, H. Riedel, and P. Neumann: *Int. Conf. on Low Cycle Fatigue and Elasto-Plastic Behaviour of Materials*, 2nd ed., Munich, Germany, 1987, pp. 277-83.
15. J. Bressers, U. Schusser, and B. Ilschner: *Int. Conf. on Low Cycle Fatigue and Elasto-Plastic Behaviour of Materials*, 2nd ed., Munich, Germany, 1987, pp. 365-70.
16. M. Karasek, H. Sehitoglu, and D. Slavik: *Low Cycle Fatigue—Directions for the Future*, Proc. ASTM Conf., Lake George, NY, Oct. 1985.
17. G.R. Halford and J.F. Saltsman: *Proc. of ASME Conf. on Thermal Stress, Material Deformation, and Thermo-Mechanical Fatigue*, H. Sehitoglu and S.Y. Zamrik, eds., ASME, New York, NY, 1987, PVP-vol. 123, pp. 9-21.
18. G.R. Halford and S.S. Manson: *Thermal Fatigue of Materials and Components*, ASTM STP 612, D. Spera and D. Mowbray, eds., 1976, pp. 239-54.
19. ASME Boiler and Pressure Vessel Code, Case N-47-23, Class 1 Components in Elevated Temperature Service, Section III, Division 1, 1986.
20. T. Bui-Quoc and A. Biron: *3rd Int. Conf. on Pressure Vessel Technology, Part II*, ASME, New York, NY, 1977, pp. 853-60.
21. M. Bernard-Connolly, A. Biron, and T. Bui-Quoc: *Trans. CSME*, 1978–79, vol. 5 (3), pp. 173-78.
22. J. Lemaitre and A. Plumtree: *J. Eng. Mater. Tech.*, Trans. ASME, 1979, vol. 101 (7), pp. 284-92.
23. A. Plumtree: *Can. Metall. Quart.*, 1979, vol. 18, pp. 197-205.
24. T. Bui-Quoc and R. Gomuc: *ASME Int. Conf. on Advances in Life Prediction Methods*, D.A. Woodford and J.R. Whitehead, eds., 1983, pp. 105-13.
25. J.L. Chaboche: in *Engineering Approaches to High Temperature Design*, B. Wilshire and D.R.J. Owen, eds., 1983, vol. 2, pp. 177-235.
26. S. Majumdar and P.S. Maiya: *J. Eng. Mater. Tech.*, 1980, vol. 102 (1), pp. 159-67.
27. S. Majumdar: *Proc. ASME Conf. on Thermal Stress, Material Deformation and Thermo-Mechanical Fatigue*, H. Sehitoglu and S.Y. Zamrik, eds., ASME, New York, NY, 1987, PVP-vol. 123, pp. 31-36.
28. J. Wareing: *Metall. Trans. A*, 1977, vol. 8A, pp. 711-21.
29. B. Tomkins: *Creep and Fatigue in High Temperature Alloys*, J. Bressers, ed., Applied Science Publishers, London, 1981, pp. 111-43.
30. C.E. Jaske: *ASME Int. Conf. on Advances in Life Prediction Methods*, 1983, pp. 93-103.
31. J.K. Tien, S.V. Nair, and V.C. Nardone: in *Flow and Fracture at Elevated Temperatures*, 1985, pp. 179-213.
32. C. Levaillant and A. Pineau: *Low-Cycle Fatigue and Life Prediction*, ASTM STP 770, 1982, pp. 169-93.
33. K.-T. Rie and R.-M. Schmidt: *Int. Conf. on Low Cycle Fatigue and Elasto-Plastic Behaviour of Materials*, 2nd ed., Munich, Germany, 1987, pp. 223-28.
34. B.K. Min and R. Raj: *Acta Metall.*, 1978, vol. 26, pp. 1007-22.
35. S. Baik and R. Raj: *Metall. Trans. A*, 1982, vol. 13A, pp. 1207-14.
36. S. Baik and R. Raj: *Metall. Trans. A*, 1982, vol. 13A, pp. 1215-21.
37. J. Morrow: *Internal Friction, Damping and Cyclic Plasticity*, ASTM STP 378, 1965, pp. 45-87.
38. M.L. Karasek: *Materials Engineering-Mechanical Behavior*, Report No. 132, College of Engineering, University of Illinois at Urbana-Champaign, Urbana, IL, Aug. 1986.
39. H. Sehitoglu and M. Karasek: *J. Eng. Mater. Tech.*, 1986, vol. 108 (4), pp. 192-98.
40. G. Ward, B.S. Hockenhull, and P. Hancock: *Metall. Trans.*, 1974, vol. 5, pp. 1451-55.

41. J.E. Forrest and P.S. Bell: *Corrosion and Mechanical Stress at High Temperatures*, V. Guttmann and M. Merz, eds., 1981, pp. 339-58.
42. N. Birks and G.H. Meier: *Introduction to High Temperature Oxidation of Metals*, Edward Arnold Publishers, London, 1983.
43. A.S. Argon, I. Chen, and C. Lau: *Creep-Fatigue-Environment Interactions*, R.M. Pelloux and N.S. Stoloff, eds., TMS-AIME, 1980, pp. 46-85.
44. D. Slavik: *Materials Engineering-Mechanical Behavior*, Report No. 134, College of Engineering, University of Illinois at Urbana-Champaign, Urbana, IL, Sept. 1986.
45. D. Slavik and H. Sehitoglu: *Proc. ASME Conf. Thermal Stress, Material Deformation, and Thermo-Mechanical Fatigue*, H. Sehitoglu and S.Y. Zamrik, eds., ASME, New York, NY, 1987, PVP-vol. 123, pp. 65-82.
46. H. Sehitoglu and J.D. Morrow: *Thermal and Environmental Effects in Fatigue: Research-Design Interface*, C.E. Jaske, S.J. Hudak, Jr., and M.E. Mayfield, eds., ASME, New York, NY, 1983, PVP-vol. 71, pp. 93-109.
47. H. Sehitoglu: *J. Eng. Mater. Tech.*, 1985, vol. 107 (7), pp. 221-26.
48. Dennis A. Boismier: M.S. Thesis, University of Illinois at Urbana-Champaign, Urbana, IL, 1988.